Rayleigh, Mie, and Tyndall scatterings of polystyrene microspheres in water: Wavelength, size, and angle dependences

Cite as: J. Appl. Phys. **105**, 023110 (2009); https://doi.org/10.1063/1.3068473
Submitted: 02 October 2008 . Accepted: 05 December 2008 . Published Online: 28 January 2009

Guang S. He, Hai-Yan Qin, and Qingdong Zheng

Rayleigh, Mie, and Tyndall scatterings of polystyrene microspheres in water: Wavelength, size, and angle dependences

Guang S. He,[a] Hai-Yan Qin, and Qingdong Zheng
The Institute for Lasers, Photonics and Biophotonics, State University of New York at Buffalo, Buffalo, New York 14260-3000, USA

(Received 2 October 2008; accepted 5 December 2008; published online 28 January 2009)

The wavelength-, size-, and angle-dependent light scattering properties of polystyrene microspheres dispersed in water are systematically investigated in a spectral range from 300 to 1300 nm and a sphere-diameter range from 20 nm to 85 μm. According to the wavelength dependence of the scattering cross section on the value of $\delta=\lambda_1/2r$, where λ_1 and $2r$ are the wavelength in the surrounding medium and the diameter of the microsphere, the light scattering behaviors can be roughly classified by three major categories. Under our considered conditions, when $\delta \geq 10$, it is termed Rayleigh scattering, characterized by a minus fourth-power dependence on the wavelength; when $10^{-2} \leq \delta \leq 10$, it is termed Mie scattering, characterized by a power factor varying within a range roughly -4 to +2; finally when $\delta \leq 10^{-2}$, it is termed Tyndall scattering, characterized by an almost constant scattering cross section that is actually independent of the wavelength. All of our experimental results on 16 scattering samples of different sizes are in good agreement with the theoretical predictions within an experimental uncertainty of $\pm 5\%$. © *2009 American Institute of Physics*.
[DOI: 10.1063/1.3068473]

I. INTRODUCTION

Light scattering is always an important research subject for both fundamental research and applications. Generally speaking, any kind of macroscopic and/or microscopic fluctuations of spatial and/or temporal properties of a given medium will cause the scattering of an incident light beam. The appearances and origins of light scattering can be various and dependent on the constituents of the medium as well as the wavelength of the incident light beam.

The pioneer of the light scattering study was Tyndall,[1] who reported the earliest experiment demonstrating the light scattering due to aerosol or dusts in the air. Another pioneer of light scattering studies was Rayleigh.[2] He theoretically investigated the scattering caused by a dielectric sphere of a size much smaller than the light wavelength and derived a famous formula showing the fourth-power inverse proportionality between the scattering intensity and the light wavelength. Furthermore, Mie[3] accomplished a more rigorous theoretical treatment based on Maxwell's equations and obtained the solutions applicable to the particles of any constituents and sizes, surrounded by a homogeneous medium. Almost at the same time, Debye[4] also published his independent theoretical work dealing with the same issue. The theoretical achievements contributed by these two scientists as well as others are generally named Mie theory of particle's scattering of light.

Here, two facts should be pointed out to avoid any possible confusion. First, even one may use above-mentioned Rayleigh formula to explain the sky's blue color, it does not mean any frequency shift between an incident monochromatic light and the scattered light. Second, for a pure gaseous or liquid medium without any foreign bodies or particles, there is also a scattering following the same wavelength dependence as given by Rayleigh formula, therefore, it is conventionally called molecular Rayleigh scattering. In this case, however, the physical origin causing the frequency-unshifted scattering in a pure gaseous or liquid medium is the density fluctuation of the molecules.[5,6] In this sense, the scattering intensity is not only determined by the molecular density but also determined by the magnitude of molecular density fluctuation, that is, the real reason why the sky is blue. In contrast, for the scattering produced by foreign particles separated by a distance much longer than the light wavelength, the scattering intensity is simply proportional to the particle number in a unit of volume.

The studies of light scattering produced by particles suspended in a homogeneous medium (such as air or water) are of great interests.[7–11] Based on these studies researchers may develop many useful methods and technical approaches to meet the application needs, such as (i) determining particles' size, shape, structure, and composition, (ii) detecting the pollution of water or air, and (iii) understanding the appearance of common materials such as milk, latex paints, and some biological tissues. This kind of studies is of special significance for meteorological optics, space optics, and lidar/radar technologies.

In the recent years, a number of research works were reported, which concerned some aspects of the light scattering investigation of polystyrene microspheres with sizes from several hundreds of nanometers to several micrometers.[12–18] One of the reasons to choose polystyrene microspheres as the scatters is that they are commercially available with well controlled shape and a broad choice of

[a]Author to whom correspondence should be addressed. Electronic mail: gshe@acsu.buffalo.edu.

sizes. In addition, the density of polystyrene (1.05 g/cm^3) is very close to that of water, so that we can have very homogeneous microsphere suspension in water without segregation or deposition during the period of measurement.

The purposes of our present work are (1) to choose polystyrene microspheres' suspension in water as a modeling sample to have systematical experimental results of the wavelength (300–1300 nm)-, size (20 nm–80 μm)-, and angle (0°–360°)-dependent scattering properties, and (2) to compare these experimental results with the calculation results predicted by the general Mie theory of particle's scattering of light. If there is a good agreement between them, then both of them can be used to predict the scattering behavior of any other particles with different constituents and sizes.

II. BASIC FORMULATION OF MIE THEORY FOR LIGHT SCATTERING

A. Scattering cross section of a dielectric sphere

The light scattering cross section of an individual dielectric sphere suspended in a homogeneous medium can be expressed as[19,20]

$$\sigma_s = \frac{\lambda_1^2}{2\pi}\sum_{n=1}^{\infty}(2n+1)(|a_n|^2+|b_n|^2). \tag{1}$$

Here, n is a positive integer and a_n and b_n are two complex coefficients defined by

$$a_n = (-1)^{n+1/2}\frac{S_n(\alpha)S_n'(\beta) - mS_n(\beta)S_n'(\alpha)}{S_n'(\beta)\phi_n(\alpha) - mS_n(\beta)\phi_n'(\alpha)},$$

$$b_n = (-1)^{n+3/2}\frac{mS_n(\alpha)S_n'(\beta) - S_n(\beta)S_n'(\alpha)}{mS_n'(\beta)\phi_n(\alpha) - S_n(\beta)\phi_n'(\alpha)}, \tag{2}$$

where $m=n_2/n_1$, n_1 and n_2 are the refractive indices of the surrounding medium and the sphere, respectively, and

$$S_n = \left(\frac{\pi z}{2}\right)^{1/2} J_{n+1/2}(z), \quad S_n'(z) = \frac{\partial S_n(z)}{\partial z},$$

$$\phi_n = S_n(z) + iC_n(z), \quad \phi_n'(z) = \frac{\partial \phi_n(z)}{\partial z},$$

$$C_n = (-1)^n\left(\frac{\pi z}{2}\right)^{1/2} J_{-n-1/2}(z), \tag{3}$$

where $J_{n+1/2}(z)$ and $J_{-n-1/2}(z)$ are Bessel functions of half-integral order and z takes on the values α or β,

$$\alpha = 2\pi r/\lambda_1, \quad \beta = m\alpha. \tag{4}$$

Here r is the radius of the sphere, $\lambda_1=\lambda_0/n_1$ is the wavelength of the incident beam in the surrounding medium, and λ_0 is the wavelength of the incident beam in vacuum.

From Eqs. (1)–(4) one can see that the scattering cross section is a function of α, β, and m, or in other words, a function of r, n_1, n_2, and λ_0.

B. Angular distribution of scattering light intensity

The angular distribution of scattering intensity from a dielectric sphere is dependent not only on the parameters mentioned above but also on the polarization status of the incident light beam. In a given observation plane containing the incident beam and the observed scattering beam, the scattering angle (θ) is defined by the angle between the propagation direction of the incident beam and the direction of the observed scattering beam. For simplicity, it is assumed that the incident beam is a linearly polarized light with its electric-vector perpendicular to the observation plane, the angular distribution of the scattering intensity from a sphere can be described as

$$i_1 = \left|\sum_{n=1}^{\infty}\frac{2n+1}{n(n+1)}(a_n\pi_n + b_n\tau_n)\right|^2. \tag{5}$$

Here a_n and b_n are given by Eq. (2), while

$$\pi_n = \frac{dP_n}{dx}, \quad \pi_n' = \frac{d^2P_n}{dx^2},$$

$$\tau_n = \pi_n x - (1-x^2)\pi_n', \tag{6}$$

where P_n is Legendre polynomial of degree n and $x=\cos(\pi-\theta)$.

Similarly, if the electric-vector direction of the incident linearly polarized beam is parallel to the observation plane, the intensity angular distribution will be

$$i_2 = \left|\sum_{n=1}^{\infty}\frac{2n+1}{n(n+1)}(a_n\tau_n + b_n\pi_n)\right|^2. \tag{7}$$

Furthermore, if the incident beam is a natural light, or linearly polarized with a polarization plane having a 45° angle to the observation plane, the angular distribution of the total scattering intensity can be expressed as

$$\bar{i} = (i_1 + i_2)/2. \tag{8}$$

C. Determination of scattering induced light attenuation

If a great number of particles are dispersed in a homogeneous medium, the attenuation of a monochromatic plane wave passing through such a medium can be described as

$$I(\lambda_0, l) = I_0(\lambda_0)e^{-K_1 l}e^{-K_2 l} = I_0(\lambda_0)e^{-K_1 l}e^{-(K_2^a+K_2^s)l}. \tag{9}$$

Here, $I_0(\lambda_0)$ is the initial intensity of the incident light, l is the propagation distance in the medium containing the particles, K_1 is the extinction coefficient of the homogeneous surrounding medium, which is mainly due to absorption; whereas K_2 is the extinction coefficient relating to the particles. Moreover, in a general case, K_2 can include two components (K_2^a and K_2^s), the former is determined by the absorption of the particles, while the latter is determined by the scattering of them. It is noted that all above-mentioned extinction coefficients are functions of the wavelength.

If the particles are nonabsorbing in the considering wavelength range, $K_2^a=0$, we have an expression for the transmittance of such a system,

$$T(\lambda_0)=\frac{I(\lambda_0,l)}{I_0(\lambda_0)}=e^{-K_1(\lambda_0)l}e^{-K_2^s(\lambda_0)l}=T_1(\lambda_0)e^{-K_2^s(\lambda_0)l}, \quad (10)$$

where $T_1(\lambda_0)$ is the transmittance of a pure homogeneous medium without the particles. In practice, if one can measure $T(\lambda_0)$ for the whole system and $T_1(\lambda_0)$ for the pure surrounding medium separately, the scattering extinction coefficient $K_2^s(\lambda_0)$ is ready to be determined through the following relationship:

$$K_2^s(\lambda_0)=\frac{1}{l}\cdot\ln\left[\frac{T_1(\lambda_0)}{T(\lambda_0)}\right]. \quad (11)$$

Furthermore, if the average distance between the particles is larger than the light wavelength, the following simple relationship between the scattering extinction coefficient and the scattering cross section (σ^s) of the particles holds:

$$K_2^s(\lambda_0)=\sigma^s(\lambda_0)\cdot N_s, \quad (12)$$

where N_s is the particle number per cm^3 and $\sigma^s(\lambda_0)$ is in units of cm^2.

From Eqs. (11) and (12) one can see that once the scattering extinction coefficient as a function of wavelength is measured, the corresponding scattering cross section of the particles as a function of wavelength can also be determined.

III. SCATTERING SAMPLES

The samples for scattering measurements are polystyrene microspheres dispersed in water. Altogether, 16 samples of microspheres with different diameters suspended in deionized water are employed for measuring the scattering cross section as a function of wavelength. The diameter, size deviation, original concentration (d_0) from the suppliers, as well as the final diluted concentration for our spectral measurements are listed in Table I. All original samples were from Polysciences, Inc. except sample Nos. 1, 2, 4, and 13 which were from Duke Scientific. Each tested sample was put in a 1 cm path-length quartz-glass cuvette for spectral transmission measurements.

As mentioned in Sec. II, in order to calculate the scattering cross section as a function of wavelength, one must know the refractive-index values as a function of wavelength for both the surrounding medium (water) and the sphere medium (polystyrene). In this work, the spectral range for reliable measurement of scattering cross section was from 300 to 1300 nm, limited by the strong absorption in IR by water. Within this spectral range, the refractive-index values at different wavelengths for water were adopted from Ref. 21, while for polystyrene the refractive-index values were given by Cauchy's dispersion formula,[22]

$$n_2(\lambda_0)=A+\frac{B}{\lambda_0^2}+\frac{C}{\lambda_0^4}, \quad (13)$$

where the constants A, B, and C are 1.5663, 0.00785, and 0.000334, respectively, when λ_0 is expressed in microns.

TABLE I. Polystyrene [polystyrene density of 1.05 g/cm^3; refractive index (589 nm at 25 °C) of 1.59] microspheres dispersed in water [water density of 1.0 g/cm^3; refractive index (589 nm at 20 °C) of 1.333] for scattering spectral measurements

Sample	Diameter ($2r$)	Standard deviation	Microspheres concentration d_0(g/ml)	Concentration after dilution d'
1	21 nm	1.5 nm	0.01	$d_0/50$
2	33 nm	1.4 nm	0.01	$d_0/100$
3	45 nm	5.3 nm	0.027	$d_0/100$
4	59 nm	2.5 nm	0.01	$d_0/200$
5	81 nm	10 nm	0.0264	$d_0/1000$
6	202 nm	10 nm	0.0259	$d_0/2000$
7	356 nm	14 nm	0.0263	$d_0/2500$
8	465 nm	11 nm	0.0265	$d_0/2500$
9	914 nm	10 nm	0.0262	$d_0/2000$
10	1.53 μm	39 nm	0.0259	$d_0/1500$
11	2.06 μm	24 nm	0.0265	$d_0/1250$
12	4.30 μm	130 nm	0.0264	$d_0/120$
13	15.2 μm	150 nm	0.0029	$d_0/7$
14	25 μm	3.7 μm	0.0268	$d_0/40$
15	43.3 μm	2.23 μm	0.0254	$d_0/10$
16	85 μm	13.6 μm	0.0259	$d_0/10$

IV. EXPERIMENTAL SETUPS AND CONDITIONS

The major experimental tasks for this study is to measure (i) the wavelength dependence of scattering cross section over the entire visible range and the near IR range and (ii) the angular dependence of the scattering intensity. After that we can give a systematic and quantitative comparison between our experimental results and the theoretical predictions based on the formation given in Sec. II.

To measure the scattering induced attenuation of our samples, as shown in Fig. 1(a), a UV-3101 PC spectrophotometer (from Shimadzu) was used for the basic measurements of transmission of the tested samples as a function of wavelength. Comparing the measured transmittance spectra of the scattering samples with that of a pure water sample of the same path length, one can determine the scattering extinction coefficient or cross section as a function of wavelength. However, in the case shown in Fig. 1(a), the detector's effective aperture of the spectrophotometer is larger than the incident beam's aperture. For this reason, when the sphere diameter is larger than the order of 1 μm, the forward scattering with small scattering angle θ becomes so dominant that partial forward scattering light can also be detected with the transmitted incident light together, which will lead to a systematic error by giving an apparently larger transmittance. To overcome this problem, a specially designed setup was employed to correct the spectral measurement results obtained by using a commercial spectrophotometer. In this case, as shown in Fig. 1(b), a Ti:sapphire laser oscillator/amplifier system (CPA-2010 from Clark-MXR) was utilized to generate a highly collimated white-light continuum beam through a 10 cm long heavy water cell.[23,24] This collimated white-light light with an ~3 mm beam size passed through the tested scattering sample and was detected at a far distance (~2 m) from the sample position by a spectrometer (EPP 2000 from StellarNet Inc.) with a charge

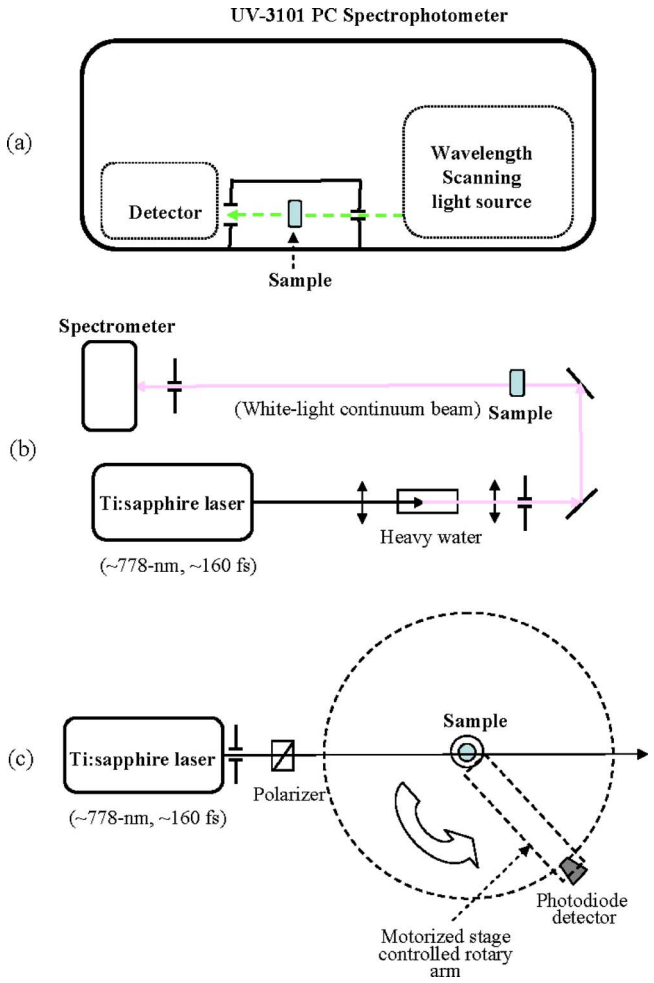

FIG. 1. (Color online) Experimental setups for (a) scattering extinction measurement using a spectrophotometer, (b) scattering extinction measurement using a collimated white-light continuum beam, and (c) angular distribution measurement of scattering light.

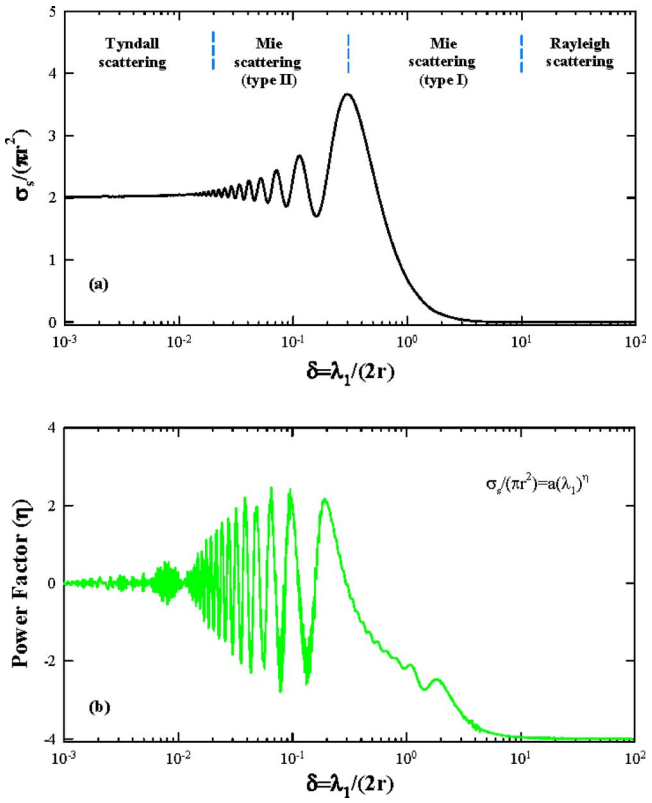

FIG. 2. (Color online) (a) Calculated curve of the relative scattering cross section vs the parameter δ; (b) calculated curve of the power factor vs the parameter δ.

coupled device array detector. To ensure that no small-angle forward scattering can enter the spectrometer, a pinhole with an aperture smaller than 3 mm was placed in front of the spectrometer. In this way the measured light attenuation as a function of wavelength is more reliable with no need of correction.

In order to measure the angular distribution of the scattering light from the samples with different sphere sizes, a setup shown in Fig. 1(c) was employed. In this case, the same Ti:sapphire laser system was utilized as the incident light source, which generated laser pulses of 778 nm wavelength, ~160 fs duration, ~3 mm beam size, ~0.22 mrad divergence angle, and 1 kHz repetition rate. The tested sample was put in a standard NMR tube made of Pyrex glass of 5 mm inner diameter. The 775 nm laser beam of pulse energy of ~25 μJ was passed through a polarizer prism, and then transversely entered the sample tube. A photodiode detector was fixed on the end of a rotating arm controlled by a motorized rotary stage working over a range of 0°–360°. The photodiode detector was connected to a Boxcar Averager (model 4420 from EG&G) by which the relative scattering intensity distribution as a function of scattering angle was recorded. To reduce the influence of the reflection from the surfaces of the NMR tube which had a relatively small diameter, the NMR tube was immersed in a dimethyl sulfoxide filled glass vial of ~25 mm diameter.

V. WAVELENGTH/SIZE DEPENDENCE

A. Particle scattering classification based on its wavelength/size dependence

Based on Eqs. (1)–(4), one knows that the scattering behavior of a microsphere is determined by two parameters, $\alpha=2\pi r/\lambda_1$ and $\beta=m\alpha$, or in other words, determined by the ratio of $\lambda_1/2r$ and the refractive indices of n_1 and n_2. Sometimes it is important for researchers to know the generalized dependence of scattering behavior on the ratio of $\delta=\lambda_1/2r$ with temporarily ignoring the detailed dispersion property of n_1 and n_2. For this purpose, the relative scattering cross section, i.e., $\sigma_s/(\pi r^2)$ is plotted in Fig. 2(a) as a function of the parameter δ, by using Eq. (1) and constant n_1 and n_2 values at 500 nm wavelength. To obtain this theoretical curve, ~1200 points are calculated and smoothed over every five points, which is based on the assumption that sphere diameter exhibits ±2.5% deviation. For a given average sphere size, the curve shown in Fig. 2(a) represents the wavelength dependence of the scattering cross section. Regardless of the variation details of this curve, the following phenomenological relationship between the cross section and the wavelength can be assumed:

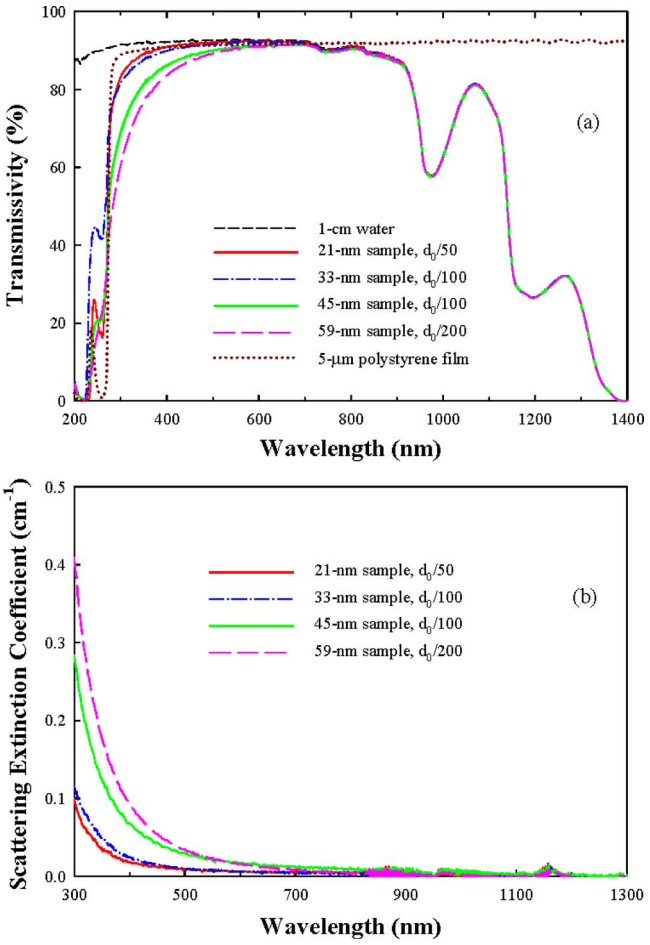

FIG. 3. (Color online) (a) Transmission spectra of a 1 cm water sample, a 5 μm polystyrene film sample, and four 1 cm scattering samples of different polystyrene sphere diameters; (b) measured scattering extinction coefficient for the above scattering samples.

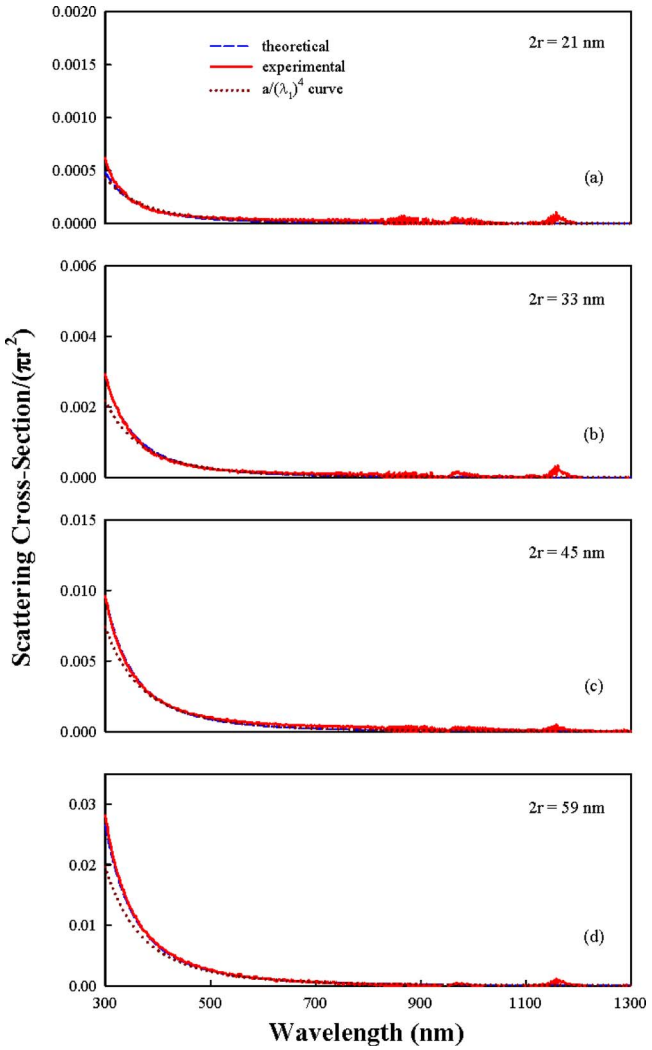

FIG. 4. (Color online) Experimental and theoretical curves of the relative scattering cross section vs the wavelength for four scattering samples with different sphere diameters: (a) 21, (b) 33, (c) 45, and (d) 59 nm.

$$\sigma_s(\lambda_1) = a \cdot \lambda_1^{\eta}, \tag{14}$$

where a is an arbitrary constant and η is a variable parameter. A logarithmic operation on both sides of the above equation leads to

$$\log[\sigma_s(\lambda_1)] = \log a + \eta \log \lambda_1, \tag{15}$$

and therefore the power factor η as a function of wavelength can be obtained after derivative operation,

$$\eta(\lambda_1) = \frac{d\{\log[\sigma_s(\lambda_1)]\}}{d[\log \lambda_1]}. \tag{16}$$

From the data of $\log[\sigma_s(\lambda_1)]$, as a function of $\log \lambda_1$, we can finally obtain the differential results shown in Fig. 2(b). Now from Figs. 2(a) and 2(b) we can see that when $\delta \geq 10$ there is an $\eta = -4$ power dependence on the wavelength, which is the same law as that the molecular Rayleigh scattering follows. This type of particle's scattering can also be termed "Rayleigh scattering," although in this case the scattering origin is different from that of the molecular scattering in a pure (gas or liquid) medium. In contrast, when $\delta \leq 10^{-2}$ the scattering cross section is essentially independent of the wavelength, and this type of scattering behavior can be termed Tyndall scattering that is characterized by a constant relative cross-section value of 2. When the ratio of δ is between these two limiting ranges, we deal with the so-called Mie scattering that can be further characterized according to Fig. 2: (i) when $\sim 0.2 \leq \delta \leq 10$ the relative cross-section value is rising monotonously with the decrease in δ, with a power factor η, varying from -4 to 0; (ii) when $10^{-2} \leq \delta \leq (\sim 0.2)$ the relative cross-section values are oscillating around the average level of value of 2.

Knowing the generalized behavior of the relative cross section as a function of the parameter $\delta = \lambda_1 / 2r$, one can choose the suitable particle's size to control the scattering behavior in the designated spectral range. If the particle size is given, one may choose suitable wavelengths to reach the expected scattering behavior. However, it should be emphasized that the discussions above only gave some rough estimations about the classifications as we did not take the dispersion influence of the refractive indices into account. More precise results of calculation with considering the refractive-index dispersion and the comparison with experimental results will be presented in Sec. V B.

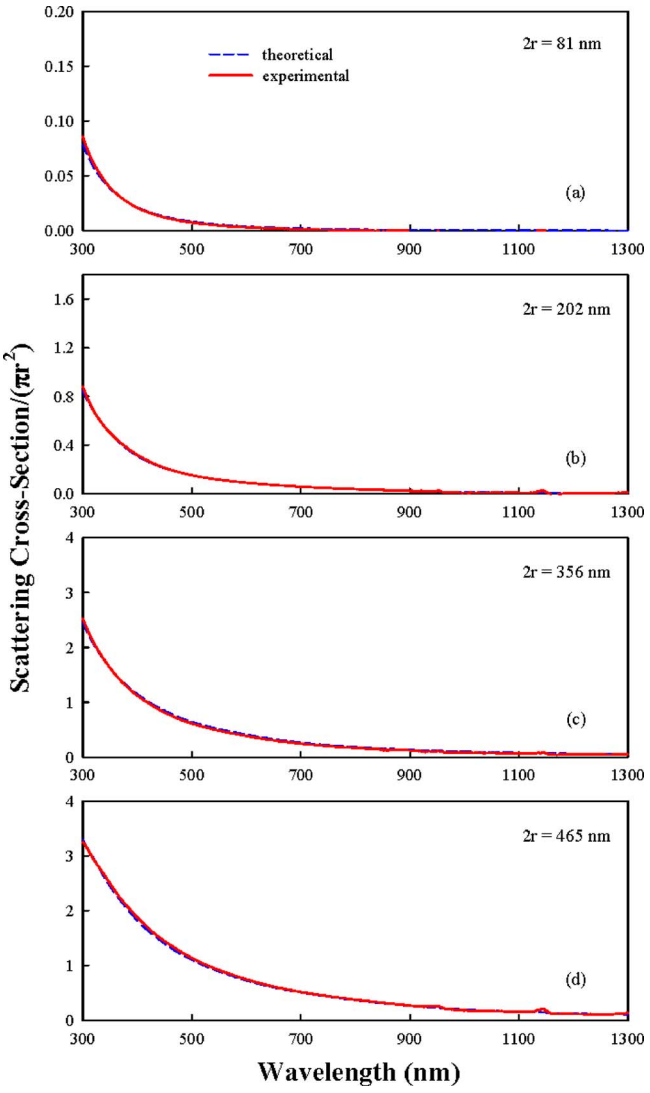

FIG. 5. (Color online) Experimental and theoretical curves of the relative scattering cross section vs the wavelength for four scattering samples with different sphere diameters: (a) 81, (b) 202, (c) 356, and (d) 465 nm.

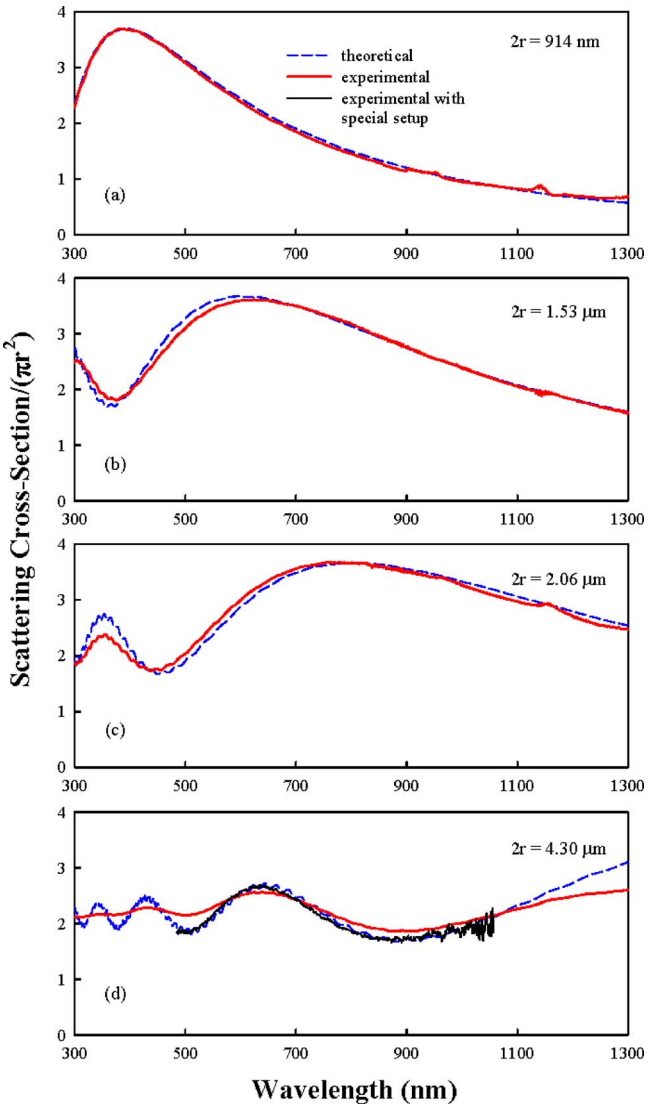

FIG. 6. (Color online) Experimental and theoretical curves of the relative scattering cross section vs the wavelength for four scattering samples with different sphere diameters: (a) 0.914, (b) 1.53, (c) 2.06, and (d) 4.30 μm.

B. Comparisons between the experimental results and the theoretical predictions

The wavelength dependence of scattering due to polystyrene microspheres with different diameters suspended in water can be determined through measuring the scattering-induced spectral transmittance changes, by using the setup shown in Fig. 1(a). As an example, shown in Fig. 3(a) are the transmission spectra of a 1 cm path-length water sample and four scattering samples of the same path length. The spheres' diameters for these samples are 21, 33, 45, and 59 nm, respectively. In the measured spectral range, the pure water sample exhibits two IR absorption bands with the peak positions at 975 and 1195 nm, while there is very strong absorption in the wavelength range longer than 1400 nm. In Fig. 3(a) the transmission spectrum of a 5 μm polystyrene film, spin coated in a 1.6 mm thick quartz-glass plate, is also given by the dotted-line curve, indicating the good transparency of the polystyrene over the entire visible range as well as the near-IR range, whereas there is a strong UV absorption nearly starting from ~300 nm position. Let $T_w(\lambda_0)$ represent the measured transmittance data of the 1 cm water sample, and $T_{w+ps}(\lambda_0)$ represents the data of a 1 cm scattering sample with a given sphere size, the scattering extinction coefficient $K^s_{ps}(\lambda_0)$ due to the polystyrene spheres can be determined [see Eq. (11)],

$$K^s_{ps}(\lambda_0) = \ln[T_w(\lambda_0)/T_{w+ps}(\lambda_0)]. \quad (17)$$

The obtained curves of scattering extinction coefficient versus wavelength are shown in Fig. 3(b) for these four scattering samples. From Fig. 3(b) one can see that the measured extinction coefficient values of these four scattering samples are increasing rapidly when the wavelength decreases from ~700 to ~300 nm. In contrast, in the same spectral range the measured transmittance curve for a 1 mm thin water sample is the same as that for a 1 cm thick water sample within the experimental uncertainty of ±0.25%, revealing that the molecular Rayleigh scattering induced attenuation for a 1 cm path-length pure water sample can be neglected within the same experimental uncertainty.

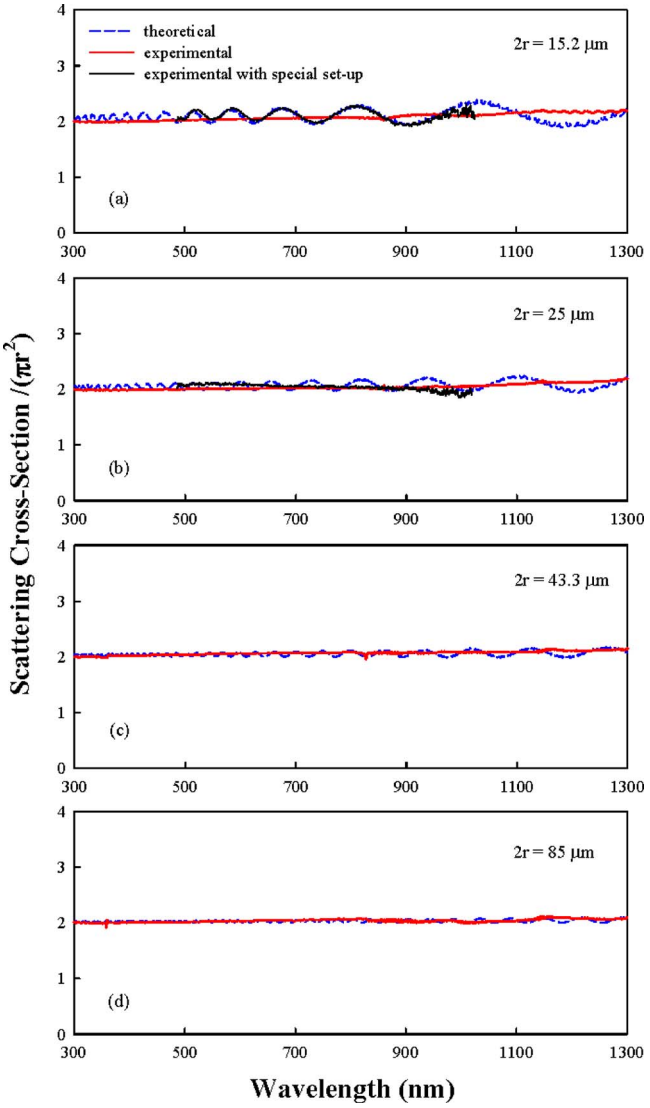

FIG. 7. (Color online) Experimental and theoretical curves of the relative scattering cross section vs the wavelength for four scattering samples with different sphere diameters: (a) 15.2, (b) 25, (c) 43.3, and (d) 85 μm.

Furthermore, knowing the weight concentration one can determine the number density (N_s) of the spheres for a given tested sample, the scattering cross section then can be obtained by using Eq. (12), i.e.,

$$\sigma^s(\lambda_0) = K^s_{\mathrm{ps}}(\lambda_0)/N_s. \tag{18}$$

Figure 4 shows such obtained cross-section curves for these four scattering samples. One can see that there is a good agreement between the experimental results and the theoretical predictions considering the refractive-index dispersion, but only for the sample of 21 nm sphere's size, the experimental curve is near-perfectly following the $1/\lambda^4$ law (characterizing the Rayleigh scattering) over the entire spectral range from 300 to 1300 nm. For other three samples with a larger spheres size, there is a gradually increased deviation from that law in the spectral range of 300–400 nm. Roughly speaking, the results presented in Fig. 4 are the examples shown the particles' Rayleigh scattering behavior at least in the spectral range of 400–1300 nm.

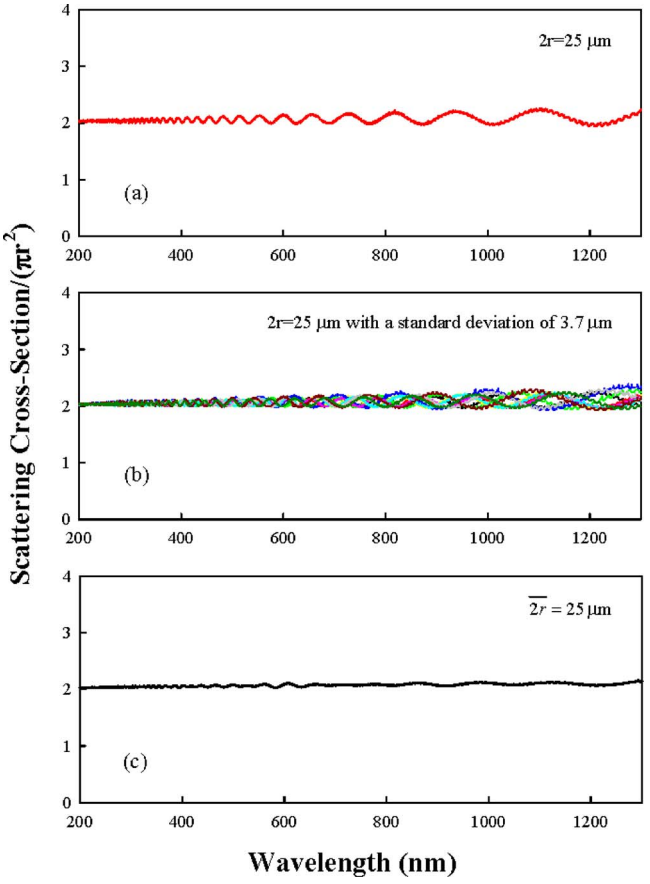

FIG. 8. (Color online) Calculated curves of the relative cross section vs the wavelength for (a) the spheres of exactly the same diameter (25 μm), (b) the group of spheres with ten different diameter values within a standard deviation of 3.7 μm around the mean value of 25 μm, and (c) the average result for the same group of spheres with an average diameter of 25 μm.

Figure 5 shows the experimental results for the second group of samples with sphere sizes of 81, 202, 356, and 465 nm, respectively. The common features of this group of data are (i) an almost perfect agreement between the experimental results and the theoretical predictions, and (ii) there is a monotonous increase in cross section following the decrease in wavelength with a power factor of $-4 \leq \eta \leq 0$ that meets the criterion of type-I Mie scattering schematically shown in Fig. 2.

Figure 6 shows the experimental results for the third group of samples with the sphere sizes of 0.914, 1.53, 2.06, and 4.30 μm, respectively. The salient feature of this group of data is that after reaching the first maximum value position, the scattering cross section manifests a damped oscillating behavior following the decrease in wavelength. In this sense, in the spectral range $\leq$700 nm the curves shown in Figs. 6(c) and 6(d) manifest the typical behavior of type-II Mie scattering.

It was found that for the tested samples with a sphere diameter of $2r \geq (1-1.5)$ μm, the cross-section values measured by using the setup shown in Fig. 1(a) became lower than the theoretical prediction. This is due to the fact that the portion of the forward scattering entered into the detector of the spectrophotometer cannot be ignored any longer. This sort of systematic errors can be corrected by using the setup

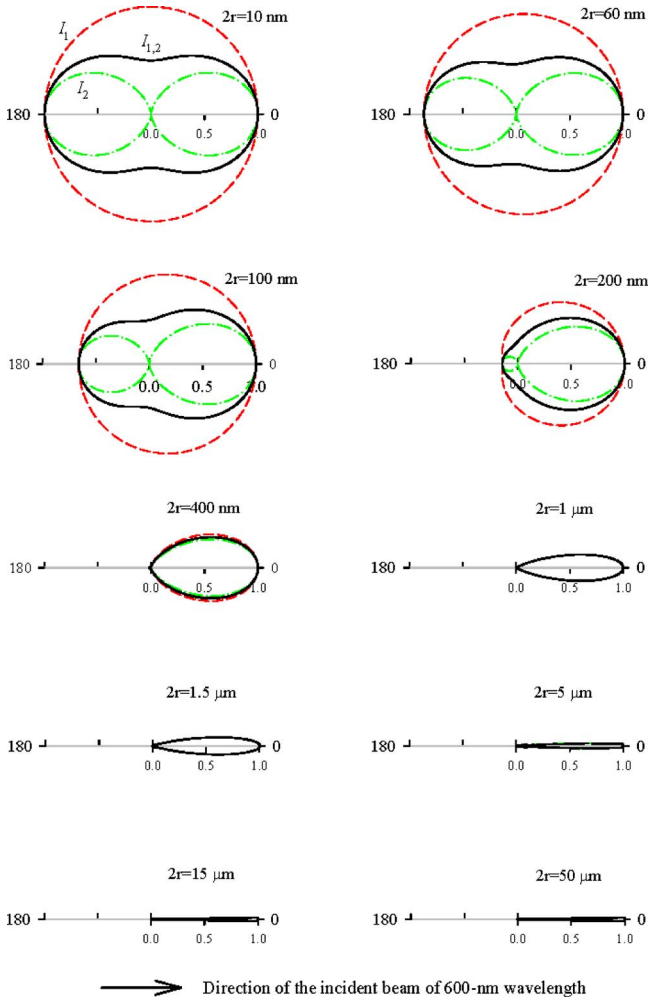

FIG. 9. (Color online) Calculated normalized angular distribution of scattering intensity for ten scattering samples with different sphere diameters. The dashed lines correspond to the incident light linearly polarized along the direction perpendicular to the observation plane, the dash-dotted lines correspond to the incident light linearly polarized in the observation plane, and the solid lines represent a natural incident light or a linearly polarized light with 45° angle to the observation plane.

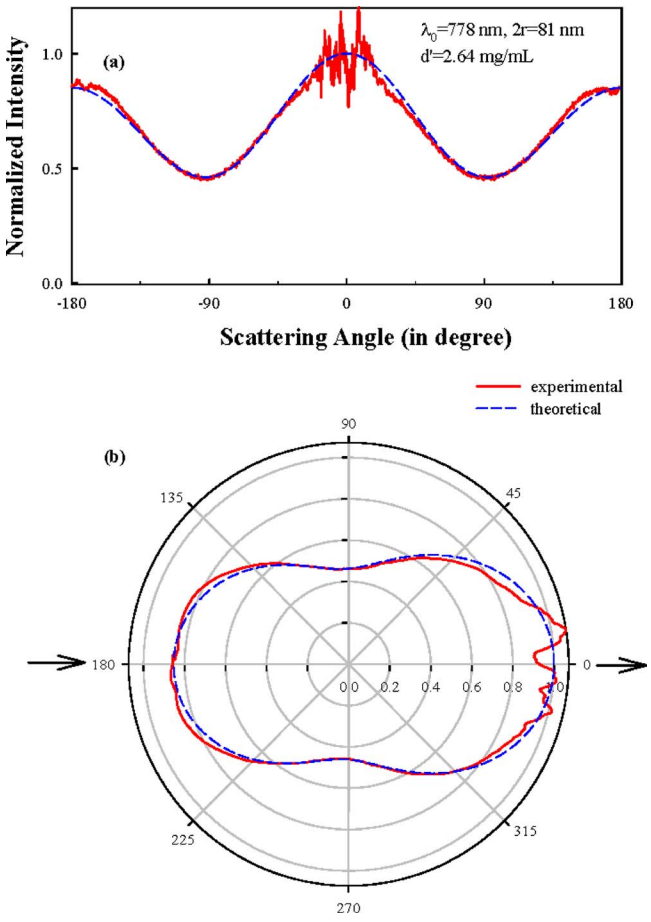

FIG. 10. (Color online) Measured and calculated angular distribution curves for the sample of $2r=81$ nm in the x-y plot (a) and the polar plot (b), respectively.

shown in Fig. 1(b), as described in Sec. IV. The thick solid lines shown in Figs. 6(b)–6(d) are the experimental curve measured by using spectrophotometer shown in Fig. 1(a) but corrected by the setup shown in Fig. 1(b) according to their peak values. One can see in Figs. 6(b) and 6(c) there is a quite good agreement between the corrected experimental curves and the theoretical predictions. However, as shown in Fig. 6(d) for the sample of $2r=4.30$ μm sample, even after correction the curve measured by the spectrophotometer is still deviated from the theoretical curve. The true experimental results measured by using a white-light continuum setup are represented by a thin solid line that is in good agreement with the theoretical curve within the spectral range from ~500 to 1000 nm, which is limited by the effectiveness of the employed white-light source. The difference between the thick-solid line and the thin-solid line curves can be explained below. In the former case, following the wavelength changes, when the forward scattering escaped into the detector of the spectrophotometer is getting stronger, the transmitted light along the original propagating direction will get weaker, as a result of summation of such two portions of contribution, the measured curve of cross section versus wavelength appears flattened.

Shown in Fig. 7 are the corresponding results obtained from the fourth group of samples with the sphere sizes of 15.2, 25, 43.3, and 85 μm, respectively. Once again, as shown in Fig. 7(a) for $2r=15.2$ μm sample, the measured results by using white-light continuum setup are in very good agreement with the theoretical prediction. However, as shown in Fig. 7(b) for the $2r=25$ μm sample, even the highly collimated white-light setup also produced a flat curve instead of an oscillating curve. This deviation is caused by another reason; it is due to the limited standard deviation of the sphere size. To explain this influence of size deviation on the resultant curve, the theoretical curve for an ideal sample containing the particles with exactly the same size of $2r=25$ μm is shown in Fig. 8(a); while a group of curves calculated with ten different diameter values within a standard deviation of 3.7 μm of a group of spheres exhibiting a mean diameter value of 25 μm are given in Fig. 8(b); finally, the resultant cross-section curve averaged over these ten components is shown in Fig. 8(c), and this curve resembles the thin solid-line curve shown in Fig. 7(b) and also is very close to the thick solid-line curve. Therefore one can say that for the cases of Figs. 7(b)–7(d), there is a typical behavior of Tyndall scattering, characterized by a nearly constant relative cross-section value of 2.

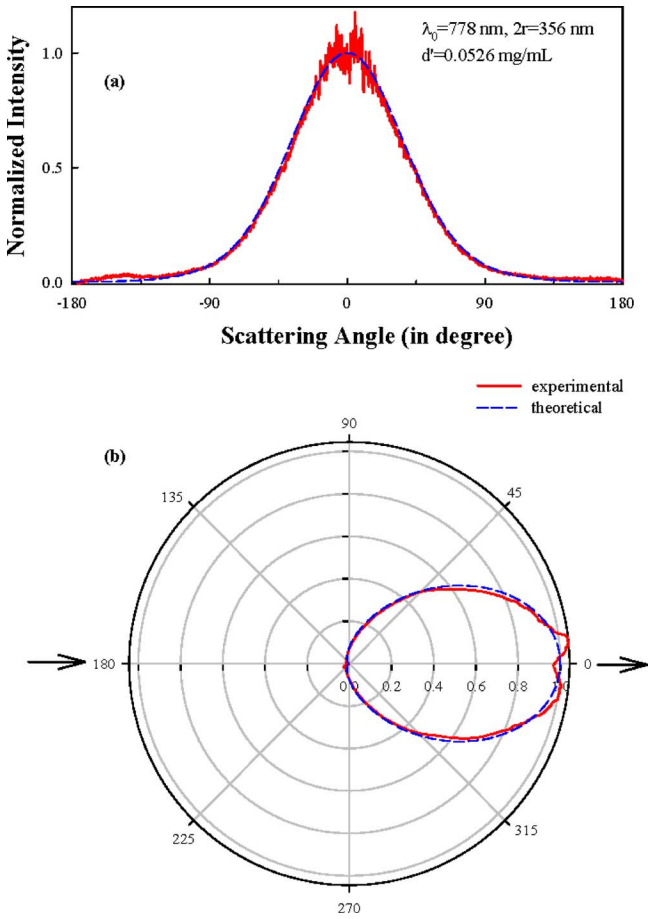

FIG. 11. (Color online) Measured and calculated angular distribution curves for the sample of $2r=356$ nm.

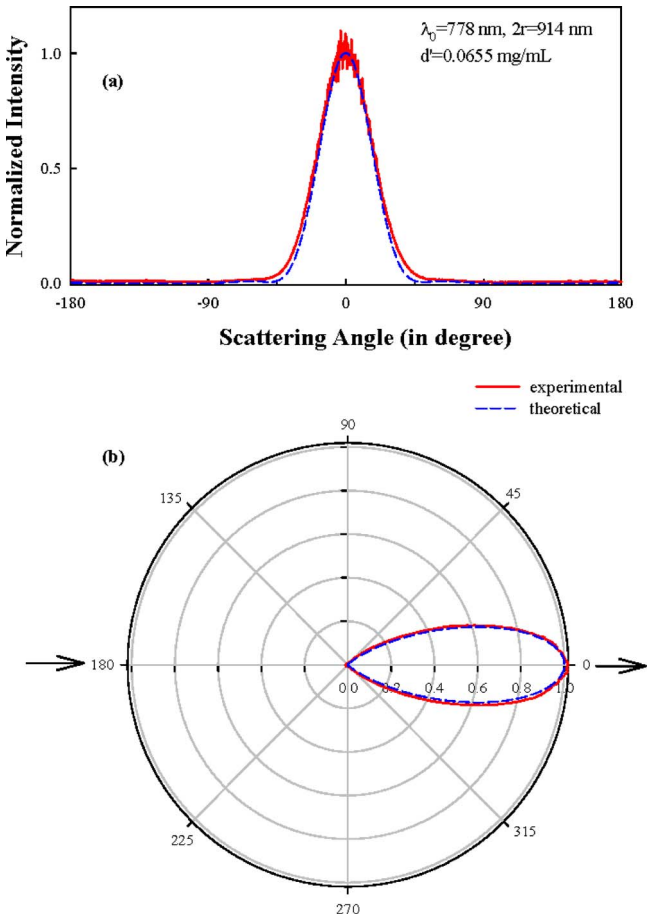

FIG. 12. (Color online) Measured and calculated angular distribution curves for the sample of $2r=914$ nm.

VI. ANGULAR DISTRIBUTION OF SCATTERING INTENSITY

Based on Eq. (5) or Eq. (7) one can determine the angular dependence of the scattering cross section if the incident light is a linearly polarized along the direction perpendicular or parallel to the observation plane. Furthermore, if the incident beam is a natural light or having two equal polarization components along these two directions, the average result is determined by Eq. (8). In practice, if the particle concentration is not too high and multiscattering effect can be neglected, the angular dependence of scattering intensity can also described by the above-mentioned three equations under the corresponding input polarization conditions.

Shown in Fig. 9 are the normalized scattering intensity distributions in a polar plot, which are calculated at $\lambda_0=600$ nm wavelength for the samples with different sphere sizes. In this figure, the dashed lines (noted by I_1) correspond to an incident beam linearly polarized along the direction perpendicular to the observation plane; the dash-dotted lines (noted by I_2) correspond to an incident beam linearly polarized along the direction parallel to the observation plane; while the thick solid lines represent the intensity distribution of $I_{1,2}=(I_1+I_2)/2$.

As shown in the first plot of Fig. 9, when the polystyrene sphere diameter $2r \leq 10$ nm, the forward and backward scattering distributions are symmetric and can be described by the same formula held by the Rayleigh scattering in a pure molecular medium, i.e.,

$$I=(1+\cos^2\vartheta)/2, \tag{19}$$

where θ is the scattering angle. When $2r \geq (20 \sim 30)$ nm, the angular distribution of scattering intensity becomes gradually asymmetric between the forward and backward directions. Moreover, when $2r \geq 200$ nm only forward scattering is dominant; furthermore, if the sphere-diameter values are greater than 5 μm, the significant scattering intensities are concentrated on a very small angular range around $\theta=0$ direction, as shown in the last three plots of Fig. 9.

In our experimental setup shown in Fig. 1(c), the incident light is a ~778 nm laser beam linearly polarized along the 45° direction with the observation plane, so that Eq. (8) can be used to calculate the angular distributions of the average scattering intensity of $I_{1,2}$.

Figure 10 shows the comparison of angular distributions between the experimental curve and theoretical curve obtained from the scattering sample of $2r=81$ nm. The solid lines and dashed lines represent the measured curves and theoretical curves and are shown in a regular x-y plot and a polar plot separately. The experimental curve shown in Fig. 10(a) consists of 2048 measured points taken by the Boxcar averager, and each point is an average result over 100 laser pulses of 1 kHz repetition rate. It is noted that the fluctuation

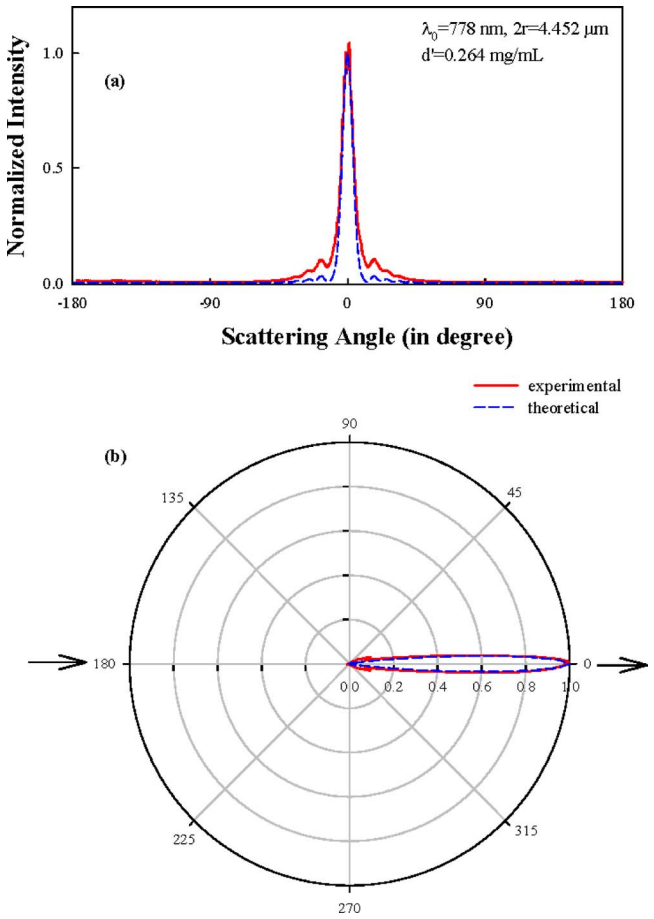

FIG. 13. (Color online) Measured and calculated angular distribution curves for the sample of $2r=4.452$ μm.

of the measured scattering signals is larger in the forward directions of smaller scattering angle. This is mainly caused by the greater influence of the diffused light signals due to the nonoptical quality of the sample tube and the surrounding glass vial. To obtain the experimental curve shown in Fig. 10(b), the original measured data are further smoothed over every 30 points.

Shown in Fig. 11 are the results for the scattering sample of $2r=356$ nm, obtained through the same way as mentioned above. It is noted that almost all scattering signals can only be observed in the half-plane of forward direction.

Figure 12 shows the similar results for the scattering sample of $2r=914$ nm with a smaller fluctuation around the peak position, and the experimental curve given in Fig. 11(b) is based on smoothing the original measured points over every 20 points.

Finally, Fig. 13 shows the angular distribution obtained for the scattering sample of $2r=4.452$ μm. In this case, the agreement between the measurements and the theoretical prediction is much better even in the forward direction with small scattering angle values, and the experimental curve shown in Fig. 13(b) is based on smoothing the original measured points over every ten points only. Nevertheless, one can see in Fig. 13(a) that in the bottoms of the two curves, there is a relatively larger deviation. We assume that it is due to the influence of the reflection from the sample tube and surrounding glass vial.

VII. CONCLUSIONS

By using three different experimental setups, we have systematically investigated the wavelength, size, and angle dependences of the scattering from polystyrene microspheres dispersed in water. Based on the dependence of scattering cross section as a function of $\lambda_1/(2r)$, the scattering behaviors can be conveniently classified by three major types (Rayleigh, Mie, and Tyndall) of particle scattering. Each type of scattering is characterized by its special wavelength dependence and angular distribution. In general, our systematical experimental results are in good agreement with the theoretical predictions given by Mie theory within an experimental uncertainty of $\pm 5\%$. This means that to a certain extent our experimental results can be useful to compare or to predict the scattering behavior of any other particles with different constituents and sizes.

ACKNOWLEDGMENTS

This work was supported by the U.S. Air Force Office of Scientific Research. H.-Y.Q. is supported by the Swedish Foundation for Strategic Research (SSF).

[1] J. Tyndall, Proc. R. Soc. London **17**, 223 (1868).
[2] L. Rayleigh, Philos. Mag. **41**, 107 (1871); **41**, 447 (1971).
[3] G. Mie, Ann. Phys. **330**, 377 (1908).
[4] P. Debye, Ann. Phys. **335**, 755 (1909).
[5] M. v. Smoluchowski, Ann. Phys. **330**, 205 (1908).
[6] A. Einstein, Ann. Phys. **338**, 1275 (1910).
[7] H. C. van de Hulst, *Light Scattering by Small Particles* (Dover, New York, 1981).
[8] C. F. Bohren and D. R. Huffman, *Absorption and Scattering of Light by Small Particles* (Wiley, New York, 1998).
[9] B. J. Berne and R. Pecora, *Dynamic Light Scattering* (Wiley, New York, 1976).
[10] B. Chu, *Laser Light Scattering* (Academic, New York, 1974).
[11] M. Kerker, *The Scattering of Light and Other Electromagnetic Radiation* (Academic, New York, 1969).
[12] E. Marx and G. W. Mulholland, J. Res. Natl. Bur. Stand. **88**, 321 (1983).
[13] S. D. T. Axford, T. M. Herrington, and B. R. Midmore, Colloids Surf. **69**, 73 (1992).
[14] A. Wax, C. Yang, R. R. Dasari, and M. S. Feld, Opt. Lett. **26**, 322 (2001).
[15] B. G. Hoover, L. Deslauriers, S. M. Grannell, R. E. Ahmed, D. S. Dilworth, B. D. Athey, and E. N. Leith, Phys. Rev. E **65**, 026614 (2002).
[16] C. E. Green, J. M. Wiencek, and M. A. Arnold, Anal. Chem. **74**, 3392 (2002).
[17] A. Petukhova, A. S. Paton, I. Gourevich, E. Kumacheva, J. J. Saarinen, and J. E. Sipe, Appl. Phys. Lett. **89**, 211908 (2006).
[18] P. N. Pinto, P. Fernandes, and R. Guerra, Meas. Sci. Technol. **18**, 1209 (2007).
[19] B. Goldberg, J. Opt. Soc. Am. **43**, 1221 (1953).
[20] M. Born and E. Wolf, *The Principles of Optics* (Pergamon, New York, 1980), Chap. 13.
[21] *Handbook of Optical Constants of Solids II*, edited by E. D. Palik (Elsevier, Boston, 1998), pp. 1067–1072.
[22] *Styrene: Its Polymers, Copolymers, and Derivatives*, edited by R. H. Boundy, R. F. Boyer, and S. M. Stoesser (Reinhold, New York, 1952), p. 524.
[23] G. S. He, T.-C. Lin, P. N. Prasad, R. Kannan, R. A. Vaia, and L.-S. Tan, Opt. Express **10**, 566 (2002).
[24] G. S. He, T.-C. Lin, J. Dai, P. N. Prasad, R. Kannan, A. G. Dombroskie, R. A. Vaia, and L.-S. Tan, J. Chem. Phys. **120**, 5275 (2004).